1 MILLION Q-FACTOR DEMONSTRATED ON MICRO-GLASSBLOWN FUSED SILICA WINEGLASS RESONATORS WITH OUT-OF-PLANE ELECTROSTATIC TRANSDUCTION

D. Senkal, M.J. Ahamed, S. Askari, and A.M. Shkel*
MicroSystems Laboratory, University of California, Irvine, CA, USA

ABSTRACT

In this paper, for the first time, we report Q-factor over 1 million, on both modes, and high frequency symmetry ($\Delta f/f$) of 132 ppm on wafer-level micro-glassblown 3-D fused silica wineglass resonators at a compact size of 7 mm diameter and center frequency of 105 kHz. In addition, we demonstrate for the first time, out-of-plane capacitive transduction on MEMS wineglass resonators. High Q-factor is enabled by a high aspect ratio, self-aligned glassblown stem structure, careful surface treatment of the perimeter area, and low internal loss fused silica material. Electrostatic transduction is enabled by detecting the spatial deformation of the 3-D wineglass structure using a new out-of-plane electrode architecture. To the best of our knowledge, work presented in this paper is the highest reported Q-factor on a degenerate mode device at 7 mm diameter or smaller. Micro-glassblowing may enable batch-fabrication of high performance fused silica wineglass gyroscopes at a significantly lower cost than their precision-machined macro-scale counterparts.

INTRODUCTION

Recently, there has been a growing interest in 3-D MEMS wineglass resonator architectures for use in inertial sensing applications due to potential advantages in symmetry, minimization of energy losses, and immunity to external vibrations [1]–[5].

Q-factor and frequency symmetry are key parameters for high performance degenerate mode Coriolis Vibratory Gyroscope (CVG) operation, as they directly relate to gyro performance metrics such as rate sensitivity, noise performance, and power consumption. However, obtaining high-Q factor and the required symmetry on 3-D MEMS devices remains to be a challenge due to factors such as thermoelastic dissipation, granularity of thin films, intrinsic material losses, high surface roughness, lack of a functional stem structure, and the associated anchor losses. Primarily, two main methods are employed in fabrication of MEMS wineglass structures: (1) deposition of thin-films on pre-defined molds, (2) blow molding the device layer into a pre-defined cavities. For example, Q-factor of 19.1k have been demonstrated on poly-silicon shell structures deposited in pre-etched cavities [1]. Q-factors up to 6.3k [2] were measured on poly-diamond wineglass shells deposited in pre-etched cavities and up to 20k were measured on sputtered ultra low expansion (ULE) glass shells deposited on precision ball lenses [3]. Blow molding was used to demonstrate Q-factors as high as 7.8k on bulk metallic glass shells [4] and 300k on fused silica shells [5].

In this paper, we explore an alternative fabrication paradigm under the hypothesis that surface tension and pressure driven micro-glassblowing process may serve as an enabling mechanism for wafer-scale fabrication of extremely symmetric and atomically smooth wineglass resonators. Micro-glassblowing process relies on viscous deformation of the device layer under the influence of surface tension and pressure forces to define the 3-D shell structure as opposed to conventional deposition, molding, or etching techniques. During the brief duration, while the device layer is still viscous, surface tension forces act on the 3-D shell structure, at an atomic level, to minimize surface roughness and structural imperfections; this leads to levels of smoothness and structural symmetry that is not available through conventional fabrication techniques. In addition, current MEMS fabrication techniques restrict the material choice to a few materials limiting the maximum achievable Q-factor. Available materials such as single-crystal silicon, have relatively high coefficient of thermal expansion (CTE) and consequently high thermoelastic dissipation (TED). Materials with low CTE, such as fused silica (0.5 ppm/°C) or ultra low expansion titania silicate glass, provide a dramatic increase in fundamental Q_{TED} limit (ULE TSG is a glass that consists of SiO_2 & TiO_2; this engineered material has the lowest known isotropic CTE of 0.03 ppm/°C). However, when compared to silicon, titania silicate glass and fused silica dry etching suffers from an order of magnitude higher surface roughness, lower mask selectivity (1:1 for KMPR photoresist), and lower aspect ratio, $<$ 6:1 [6]. Micro-glassblowing allows the use of fused silica material on a wafer-level without the need for these challenging dry etching techniques.

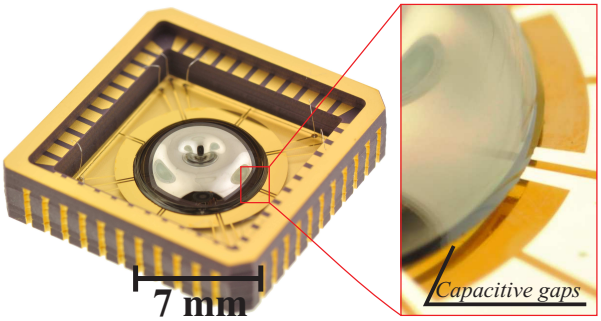

Figure 1: 1 million Q-factor fused silica wineglass structure presented in this paper (left), close-up of capacitive gaps (right).

Micro-glassblowing of borosilicate glass spherical shell structures has been demonstrated for nuclear magnetic resonance applications [7]. Later, fused silica and ultra low expansion glass micro-glassblowing of inverted-wineglass structures has been demonstrated at temperatures as high as 1700 °C [8]. Assembled electrode structures and a piezo-pinger setup were developed in [9] for electrostatic and mechanical excitation of micro-glassblown structures. Finite element analysis of the micro-glassblowing process [10], and further improvement in the fabrication process led to frequency splits (Δf) as low as $<$ 1 Hz on borosilicate glass wineglass structures [11].

In this work, we report the most recent developments in the wafer-level, micro-glassblowing paradigm for fabrication of 1 million Q-factor, highly symmetric ($\Delta f/f$ = 132 ppm) fused silica wineglass resonators at 7 mm diameter and first demonstration of out-of-plane electrostatic transduction on MEMS wineglass resonators, Fig 1.

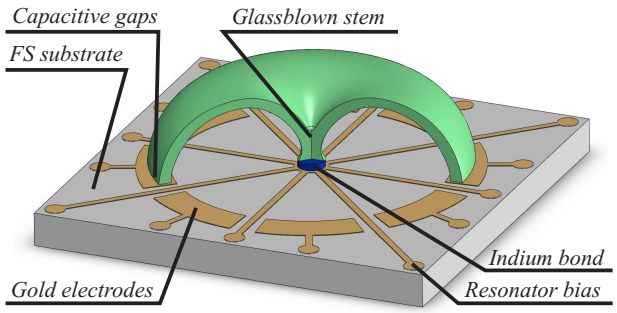

Figure 2: Out-of-plane electrode architecture consists of a micro-glassblown fused silica wineglass resonator and planar Cr/Au electrodes defined on fused silica, enabling batch-fabrication.

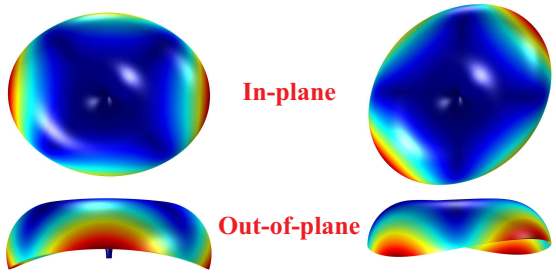

a) 1st n=2 wineglass mode *b) 2nd n=2 wineglass mode*

Figure 3: Out-of-plane transduction scheme utilizes out-of-plane component of wineglass modes to drive and sense in-plane motion.

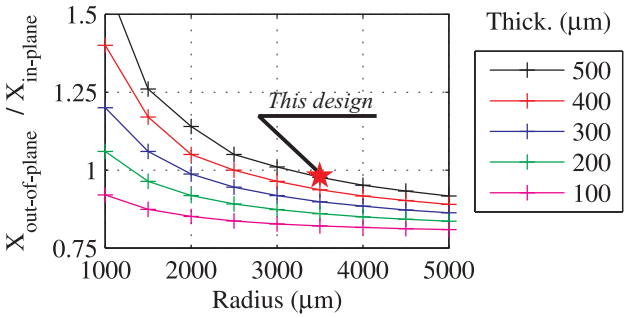

Figure 4: Out-of-plane to in-plane displacement ratio for mushroom resonators: Due to the 3-D nature of the resonator, the ratio is close to 1:1. Star marks the design presented in this paper.

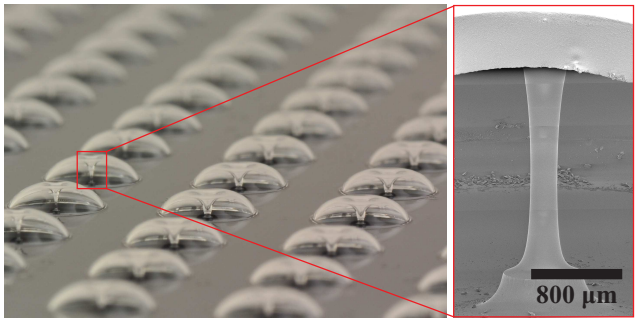

Figure 5: Array of micro-glassblown wineglass structures (left), glassblown self-aligned stem structure (right).

DESIGN

Out-of-plane electrode architecture and parameters affecting Q-factor are discussed in this section.

Out-of-plane electrode architecture

Wineglass coriolis vibratory gyroscopes typically utilize 8 or more electrodes to drive and sense the primary wineglass modes. One of the main challenges of fabricating micro-wineglass resonators is the definition of the electrode structures in a manner compatible with batch-fabrication. 3-D side-walls of the wineglass geometry makes it challenging to fabricate radial electrodes with small capacitive gaps and to keep the gap uniform across the height of the structure. Even though post-fabrication assembly techniques have been successfully demonstrated [9], these approaches create a bottle-neck in batch-fabrication of the devices at wafer level.

In this paper, we explore an alternative transduction paradigm based on out-of-plane electrode architecture. Out-of-plane electrode architecture consists of a micro-glassblown fused silica wineglass resonator and planar Cr/Au electrodes defined on a fused silica substrate, Fig. 2. Out-of-plane capacitive gaps are formed between the Cr/Au metal traces and the perimeter of the wineglass resonator. Electrostatic transduction is made possible by the 3-D mode shape of the wineglass resonator: in-plane deformation of wineglass modes is accompanied by an out-of-plane deformation, Fig. 3. This permits the use of out-of-plane transduction to drive and sense the in-plane oscillations, which are sensitive to coriolis forces along the z-axis of the structure [12]. This kind of electrode structure has several advantages over radial electrode structures:

- Even though a smaller surface area is utilized for capacitive gaps compared to radial electrodes, planar nature of the electrode structure makes it easier to obtain smaller capacitive gaps, which helps compensate for the loss of surface area.
- Sacrificial layers and wafer-to-wafer bonding techniques can be used to define the capacitive gaps, which makes the process very robust to alignment errors, as the gap uniformity is defined by the thickness of the sacrificial layer and not the wafer to resonator alignment accuracy.
- The metal traces for the electrodes can be defined on the same material used for the resonator (i.e. fused silica), providing uniform coefficient of thermal expansion between the electrode die and the resonator.
- For mushroom type geometries the ratio of out-of-plane motion to in-plane motion is close to 1:1, leading to very efficient out-of-plane transduction, Fig. 4.

Optimization of Q-factor

Total Q-factor of the vibratory structure can be calculated from contribution of individual dissipation mechanisms in a manner analogous to solving a parallel resistor network, Eq. 1. For this reason the total Q-factor is dominated by the dissipation mechanism with the lowest Q-factor (weakest link).

$$Q_{total}^{-1} = Q_{visc}^{-1} + Q_{anchor}^{-1} + Q_{mat}^{-1} + Q_{surf}^{-1} + Q_{etc}^{-1} \,. \quad (1)$$

In order to optimize the Q-factor all loss mechanisms affecting the system need to be individually addressed:

- Viscous damping, Q_{visc}, is the most dominant affect with Q-factor of several thousands at atmospheric conditions.

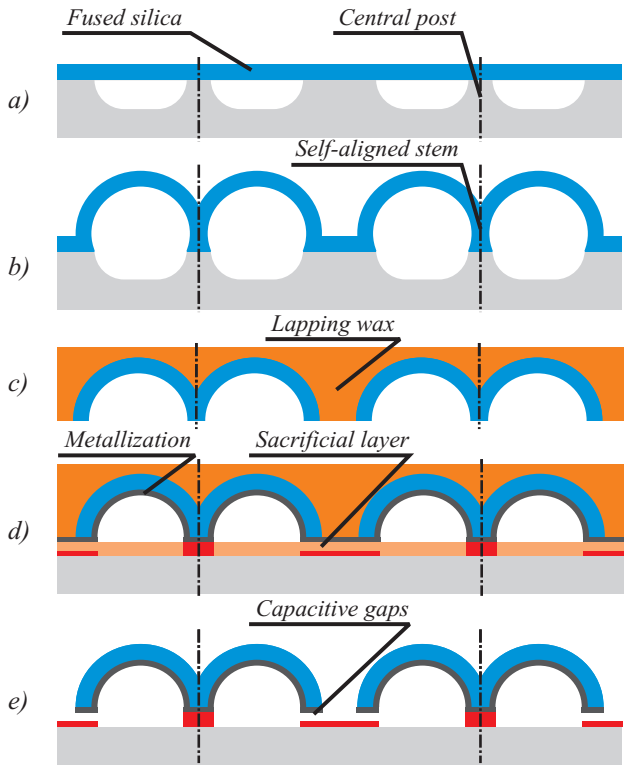

Figure 6: Wafer-level fabrication process for fused silica micro-wineglass structures.

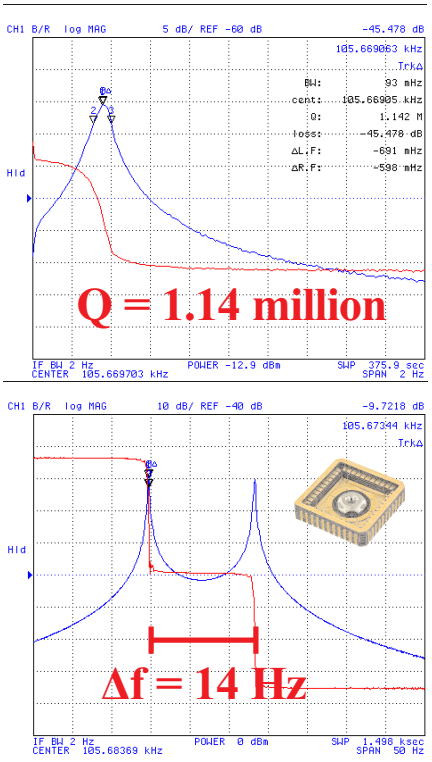

Figure 7: Frequency sweep revealed a Q-factor of 1.14 million and as fabricated freq. split (Δf) of 14 Hz at 105 kHz center freq.

However, it can easily be eliminated by operating the device in moderate to high vacuum.

- Anchor losses, Q_{anchor}, are caused by acoustic losses into the substrate and are minimized by decoupling the resonator and the substrate through a self-aligned, solid stem structure, Fig. 5.
- Material losses, Q_{mat}, can be divided into several individual loss mechanisms. Thermoelastic dissipation is caused by an interaction between the thermal fluctuations and mechanical oscillations and is minimized by using materials with low coefficient of thermal expansion (CTE), such as fused silica (0.5 ppm/°C). Additional material losses are caused by microscopic effects, such as presence of foreign materials within the matrix of the resonator material and lattice defects at grain boundaries [13]. These effects are minimized by using a high purity, isotropic fused silica material.
- Surface losses, Q_{surf}, are mainly caused by high surface roughness and metallization losses [13]. These effects are minimized through atomically smooth surfaces of micro-glassblown structures [8] and keeping the thickness of the metal layer very small with respect to the resonator shell thickness (50 nm of sputtered Iridium).
- Additional loss mechanisms, Q_{etc}, such as Akheiser dissipation have typically very high Q-factors at kHz range and are not taken into account [14].

FABRICATION

Micro-glassblowing is a wafer-level process, Fig. 5, which utilizes surface tension and pressure forces to minimize surface roughness and structural asymmetries (Δf) [11]. Fabrication process starts with $\sim 2\ \mu$m thick LPCVD poly-silicon deposition on 1 mm thick fused silica wafers. The poly-silicon mask is used to etch hemi-toroidal cavities into fused silica wafers down to $\sim 300\ \mu$m depth. The next step of the fabrication process is plasma assisted fusion bonding of a 500 μm thick fused silica device layer (Corning 7980), Fig 6(a) [8]. The wafer stack is later glassblown at $> 1600\ ^{\circ}C$ for ~ 2 minutes and rapidly cooled to room temperature, Fig 6(b). During glassblowing the device layer at the central post merges to create a solid, self-aligned stem structure, critical for high-Q operation, Fig. 5. This is followed by back-lapping the wafer stack to release the inverted wineglass structures using an Allied Multiprep 12" lapping system, Fig 6(c). A series of diamond lapping films with descending grit size of $30\ \mu\text{m} \Rightarrow 6\ \mu\text{m} \Rightarrow 3\ \mu\text{m} \Rightarrow 1\ \mu\text{m} \Rightarrow 0.5\ \mu\text{m} \Rightarrow 0.1\ \mu\text{m}$ are used for lapping, final polish is done using polishing cloth and 50 nm colloidal suspension to obtain optical polish at the perimeter of the shell structure.

Interior surface of the wineglasses is metallized with 50 nm thick sputtered Iridium on a two axis planetary stage for film uniformity. For the out-of-plane electrode structures, separate fused silica wafers are patterned with Cr/Au (100 nm / 500 nm) electrodes and coated with a thin layer of photo-resist sacrificial layer. Subsequently, lapped and metalized wineglass wafer is bonded to the out-of-plane electrode wafer at the stem of each wineglass using low out-gassing epoxy, Ablebond JM7000, Fig 6(d). Once the bonding is complete, the sacrificial layer is removed to release the inverted wineglass structures around their perimeter, creating capacitive gaps between the metalized inverted wineglass structures and the Cr/Au electrodes, Fig 6(e).

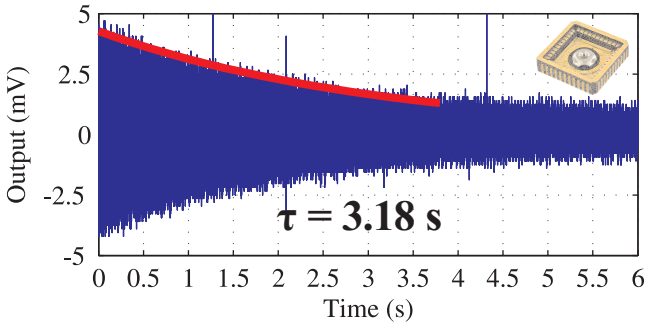

Figure 8: Ring-down experiment at 19 μTorr shows τ = 3.18 s, giving 1.05 million Q-factor at 105 kHz, confirming the sweep.

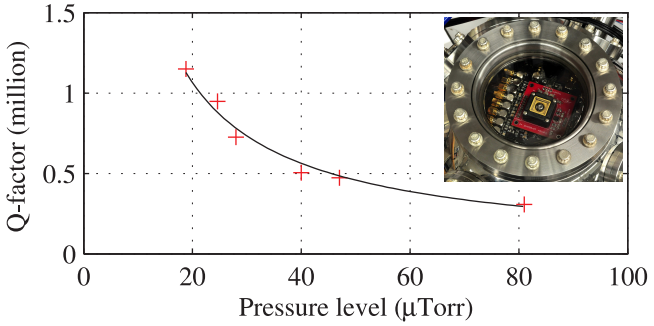

Figure 9: Q-factor vs pressure level experiment. Q-factors above 1 million were obtained after pumping down to 20 μTorr.

EXPERIMENTAL RESULTS

Frequency sweep using out-of-plane electrodes revealed Q-factor of 1.14 million and frequency split of 14 Hz at a center frequency of 105 kHz ($\Delta f/f$ = 132 ppm), Fig. 7. A separate ring down experiment was performed where the device was excited with a narrow bandwidth swept sine-wave impulse and resonator output during free vibration was recorded. Ring down experiment demonstrated a time constant of 3.18 seconds and Q-factor of 1.05 million, confirming the frequency sweeps, Fig. 8. In order to observe the effect of viscous damping on the overall Q-factor, the frequency sweep was repeated at different pressure levels. Q-factor of 1 million was obtained below < 20 μTorr, Fig. 9. No further improvement in Q-factor was observed below < 20 μTorr.

CONCLUSIONS

Micro-glassblown fused silica wineglass resonators with out-of-plane electrode structures have been fabricated. Q-factor over 1 million, on both modes, and high frequency symmetry ($\Delta f/f$) of 132 ppm have been experimentally demonstrated at a compact size of 7 mm diameter. In addition, out-of-plane capacitive transduction on MEMS wineglass resonators have been demonstrated for the first time.

To the best of our knowledge, work presented in this paper is the highest reported Q-factor on a degenerate mode device at 7 mm diameter or smaller. Low internal dissipation of fused silica combined with high structural symmetry of MEMS micro-glassblowing paradigm may enable batch-fabrication of high performance fused silica wineglass gyroscopes on a wafer surface at a significantly lower cost than their precision-machined macro-scale counterparts.

ACKNOWLEDGEMENTS

This material is based upon work supported by DARPA grant W31P4Q-11-1-0006 (Program Manager Dr. Robert Lutwak).

REFERENCES

[1] P. Shao, V. Tavassoli, L. Chang-Shun, L. Sorenson, and F. Ayazi, "Electrical characterization of ALD-coated silicon dioxide micro-hemispherical shell resonators," in *IEEE MEMS*, San Francisco, CA, USA, 2014, pp. 612–615.

[2] A. Heidari, M. Chan, H.-A. Yang, G. Jaramillo, P. Taheri-Tehrani, P. Fonda, H. Najar, K. Yamazaki, L. Lin, and D. A. Horsley, "Micromachined polycrystalline diamond hemispherical shell resonators," in *Solid-State Sensors, Actuators, and Microsystems Workshop (TRANSDUCERS)*, Barcelona Spain, 2013, pp. 2415–2418.

[3] Y. Xie, H. C. Hsieh, P. Pai, H. Kim, M. Tabib-Azar, and C. H. Mastrangelo, "Precision curved micro hemispherical resonator shells fabricated by poached-egg micro-molding," in *IEEE Sensors*, Taipei, Taiwan, 2012, pp. 279–283.

[4] M. Kanik, P. Bordeenithikasem, J. Schroers, D. Kim, and R. T. M'Closkey, "Microscale Three-Dimensional Hemispherical Shell Resonators Fabricated from Metallic Glass," in *IEEE ISISS*, Laguna Beach, CA, 2014, pp. 9–12.

[5] J. Cho, J. Yan, J. A. Gregory, H. Eberhart, R. L. Peterson, and K. Najafi, "High-Q fused silica birdbath and hemispherical 3-D resonators made by blow torch molding," in *IEEE MEMS*, Taipei, Taiwan, 2013, pp. 177–180.

[6] M. J. Ahamed, D. Senkal, A. A. Trusov, and A. M. Shkel, "Deep NLD plasma etching of fused silica and borosilicate glass," in *IEEE Sensors*, Baltimore, Maryland, USA, 2013, pp. 1767–1770.

[7] E. J. Eklund and A. M. Shkel, "Self-inflated micro-glass blowing," *US Patent 8,151,600*, 2012.

[8] D. Senkal, M. J. Ahamed, A. A. Trusov, and A. M. Shkel, "High temperature micro-glassblowing process demonstrated on fused quartz and ULE TSG," *Sensors and Actuators A: Physical*, vol. 201, pp. 525–531, Dec. 2012.

[9] D. Senkal, M. J. Ahamed, A. A. Trusov, and A. M. Shkel, "Adaptable test-bed for characterization of micro-wineglass resonators," in *IEEE MEMS*, Taipei, Taiwan, 2013.

[10] D. Senkal, M. J. Ahamed, and A. M. Shkel, "Design and Modeling of Micro-glassblown Inverted-wineglass Structures," in *IEEE ISISS*, Laguna Beach, CA, 2014, pp. 13–16.

[11] D. Senkal, M. J. Ahamed, A. Trusov, and A. M. Shkel, "Achieving Sub-Hz Frequency Symmetry in Micro-Glassblown Wineglass Resonators," *Journal of Microelectromechanical Systems*, vol. 23, no. 1, pp. 30–38, 2014.

[12] A. Renault and P. Vandebeuque, "Hemispherical resonator with divided shield electrode," *US Patent 6,945,109*, 2005.

[13] B. S. Lunin, "Physical and chemical bases for the development of hemispherical resonators for solid-state gyroscopes," *Moscow Aviation Institute, Moscow*, 2005.

[14] S. Chandorkar, M. Agarwal, R. Melamud, R. N. Candler, K. E. Goodson, and T. W. Kenny, "Limits of quality factor in bulk-mode micromechanical resonators," in *IEEE MEMS*, Tucson, AZ, USA, 2008, pp. 74–77.

CONTACT

* D. Senkal, tel: +1-949-945-0858; doruksenkal@gmail.com